The Cryosphere Discuss., 5, 1089–1122, 2011
www.the-cryosphere-discuss.net/5/1089/2011/
doi:10.5194/tcd-5-1089-2011

The Cryosphere Discussions

The evolution of the western rift area of the Fimbul Ice Shelf, Antarctica

A. Humbert[1] **and D. Steinhage**[2]

[1]Institute of Geophysics, KlimaCampus, University of Hamburg, Bundesstraße 55, 20146 Hamburg, Germany
[2]Alfred Wegener Institute for Polar and Marine Research, Am Alten Hafen 26, 27568 Bremerhaven, Germany

Received: 25 March 2011 – Accepted: 3 April 2011 – Published: 11 April 2011

Correspondence to: A. Humbert (angelika.humbert@zmaw.de)

Published by Copernicus Publications on behalf of the European Geosciences Union.

Abstract

This paper studies the evolution of a zone in the Fimbul Ice Shelf that is characterised by large crevasses and rifts west of Jutulstraumen, an outlet glacier flowing into Fimulisen. High-resolution radar imagery and radio echo sounding data were used to study the surface and internal structure of this rift area and to define zones of similar characteristics. The western rift area is dominated by two factors: a small ice rumple that leads to basal crevasses and disturbs the homogeneity of the ice, and a zone with fibre-like blocks. Downstream of the rumple we found down-welling of internal layers and local thinning, which we explain as a result of basal crevasses due to the basal drag at the ice rumple. North of Ahlmannryggen the ice looses its lateral constraint and forms individual blocks, which are deformed like fibres under shear, where the ice stream merges with slower moving ice masses of the western side. There, the ice looses its integrity, which initiates the western rift system. The velocity difference between the slow moving western part and the fast moving extension of Jutulstraumen produces shear stress that causes the rifts to form tails and expand them to the major rifts of up to 30 km length.

1 Introduction

Fimbulisen is an ice shelf fringing Dronning Maud Land, East Antarctica, located from 71.5° S to 69.5° S and 3° W to 7.5° E (Fig. 1). With a size of ~39 400 km^2 it is the largest ice shelf in the Håkon VII Sea. The ice stream Jutulstraumen, the largest outlet glacier in Dronning Maud Land, feeds the central part of the ice shelf. The inflow of this fast ice stream (about 700 ma^{-1}) divides the ice shelf into a fast and two slow moving parts and builds up an ice tongue at the calving front, the Trolltunga. As a consequence of the accumulation of cold ice in the interior of the ice sheet and the large flow velocities of Jutulstraumen, the advection leads to a bulk mass of cold ice in along the ice stream and warmer ice masses in the slow moving areas (Humbert, 2010).

TCD
5, 1089–1122, 2011
The rift zone of the Fimbul Ice Shelf
A. Humbert and D. Steinhage

A temperature profile measured in the center of the fast flowing part about half way between grounding line and ice shelf edge shows that the ice in the lower half of the ice shelf is approximately −27 °C and thus about ten degrees colder than at the surface (Orheim et al., 1990a,b).

The junction of fast and slow moving flow units contributes to shear stress. Along the eastern margin of the ice stream, this builts a classical shear margin with a field of densely distributed small cracks at the surface. The western part of Fimbulisen on the other hand, consists of an extensive field of large and wide crevasses and rifts, as satellite and airborne images show. Radar imagery, penetrating the ice surface up to several metres depth reveal even more structures, that are not visible in optical imagery. Figure 2a shows an overview of this crevasse and rift area, which we denote western rift area of Fimbulisen. This area covers a size of approximately 30 km width and 100 km length.

The existence of the western rift area presumably also plays a role in large calving events of Fimbulisen. In 1967 the entire ice tongue calved off and formed an about 5000 km^2 large iceberg, which drifted 13 yr through the Weddell Sea (McClain, 1978; Vinje, 1975; Swithinbank et al., 1977). Although the calving of Trolltunga was suggested to be triggered by a collision of an iceberg originating from the Amery Ice Shelf, the cause of the calving is rather the rifting perpendicular to the western margin of the ice front of the tongue. Vinje (1975) compares the shape of Trolltunga in 1959 and as iceberg in 1973, showing that two rifts existing already in the late fifties remained on the calved Trolltunga. These rifts were documented in the flights of the Norwegian Antarctic Expedition 1956–1960 and are likely to have evolved from the western rift zone this paper is subjected to.

This study aims to investigate the origin of the western rift area and to explain the structures found in radar imagery and radio echo sounding (RES). To this end, high-resolution radar imagery are used to define areas with similar surface characteristics. In order evaluate if the surface characteristics are linked to flow units in the vertical, radio echo sounding data was analysed and used to classify these units. Finally, the

Discussion Paper | Discussion Paper | Discussion Paper | Discussion Paper |

TCD

5, 1089–1122, 2011

The rift zone of the Fimbul Ice Shelf

A. Humbert and D. Steinhage

identified areas were incorporated in a numerical flow model to check the completeness of the classification and to investigate the softening effect of the damage. The latter part goes beyond the scope of this paper and will thus not be discussed here.

2 Database

The database consists of radar satellite imagery, as well as airborne radio echo sounding data, which are all described in detail below. Radar imagery is used to identify locations at which the internal structure of the ice is analysed using airborne radio echo sounding. At one location we additionally use a single optical image for comparison, however we do not discuss ASTER imagery as a separate part of the database.

2.1 TerraSAR-X high resolution radar imagery

We used high resolution radar imagery obtained by the X-Band Synthetic Aperture Radar TerraSAR-X. TerraSAR-X stripmap mode images acquired between 2008 and 2010 were geolocated using high-precision orbit parameters, leading to sub-pixel position accuracy (Fritz and Eineder, 2009). We assembled a mosaic with a resolution of 12.5 m from ScanSAR and stripmap mode scenes, which is shown in Fig. 1.

The penetration of the X-band radar into snow is often considered as a disadvantage, as the definite penetration depth is unknown. In our case, the penetration of the radar signal into the firn is an advantage, as it leads to an integrated signal over a shallow layer and hence provides more information than a surface signal. The scattering of the radar wave in firn can be separated into two contributions: surface scattering and volume scattering. Diffusive and specular scattering builds the surface scattering and hence, the scattering depends on the surface roughness and moisture. In dry snow, the radar wave penetrates through the surface layer and volume scattering at inhomogeneities, as well as scattering along internal boundaries of layers of different density, becomes the dominating factor. Davis and Poznyak (1993) observed a penetration

TCD
5, 1089–1122, 2011

The rift zone of the Fimbul Ice Shelf

A. Humbert and D. Steinhage

depth of a 10 GHz signal in firn of the East Antarctic cold and dry plateau region of 4.7 m. Rott et al. (1993) found for 10.3 GHz a penetration depth of 8.1 m in a dry snow zone in western Dronning Maud Land. In April 2005 during the SVALEX campaign, DLR's airborne E-SAR system was flown above the summit region of the Austfonna ice cap, Svalbard. Acquired single pass interferometric SAR data covering on-ground deployed corner reflectors as well as on site gained snow/firn profiles were utilized to estimate the X-Band penetration depth. The snow/firn profiles reveal very thin ice layers or very thin ice lenses indicating no perfect dry snow zone (R. Metzig (DLR), personal communication, 2011). The scattering volume depth for the 9.6 GHz VV polarisation radar signal was estimated to be about 16.2 m; the depth of the scattering phase center was determined to be approximately 4.5 m for this location (R. Scheiber (DLR), personal communication, 2011). For the TerraSAR-X 9.65 GHz radar signal we consider a penetration depth of 8–10 m to be realistic for the dry snow zone.

The TerraSAR-X mosaic was used to define areas with similar surface and near-surface structure. The structural characteristics are rift patterns, flow patterns and the absence of texture. The structural mapping was performed between 2.5° W and 7.5° E, however, we focus here on the area up to 1° E. The obtained zones of similar surface characteristics allow nevertheless only a two dimensional assignment. In order to asses if the surface structure allows to map units of similar internal structure, the vertical structure was explored along already available airborne RES profiles.

2.2 Airborne Radio Echo Sounding

All RES flights used in this study, were performed by the Alfred Wegener Institute between 1996 and 2008 with a radio echo sounding system developed at the TU Hamburg-Harburg for application in polar regions. The radar has a centre frequency of 150 MHz and a selectable transmitted pulse length of 60 ns or 600 ns, resulting in a vertical resolution of approximately 5–10 m (60 ns), respectively 50 m (600 ns). The short pulse allows to study the internal structure of ice sheets and shelves along the flown transects. For details on the RES system see Nixdorf et al. (1999). The horizontal

TCD
5, 1089–1122, 2011

resolution after a tenfold stack was typically 70 m. Beside stacking, the data were filtered, an amplitude correction, and a static correction were applied.

As most flights above Fimbulisen were carried out for a geophysical survey mapping magnetic and gravity field. Especially the western part of the ice shelf is covered by two regular partly overlapping flight patterns with a line spacing of 10 km. In sum 70 profiles with a total length of 11 580 km are available over the ice shelf for extraction of the ice thickness. Twenty-two of these profiles were acquired with using the 60 ns pulse and 48 with 600 ns. The resulting ice thickness dataset of Fimbulisen is based on roughly 63 500 data points. Therefore the ice thickness is well known and the gradients in thickness, e.g. close to the inflow of the ice stream are well documented. The transformation from two way travel time to ice thickness was made by using a radar velocity of $0.17\,\mathrm{m\,ns^{-1}}$ plus 8.8 m in order to account for the higher velocities in firn. The ice thickness obtained from all available RES profiles is displayed colour coded along the profiles on top of on TerraSAR-X image for the western part of the ice shelf in Fig. 2b and discussed below.

For the purpose of understanding the internal structure of the ice shelf, all twenty-three 60 ns pulse profiles and a single one with 600 ns pulse length that covers the northernmost part of Trolltunga were analysed, as there is no 60 ns pulse profile available in that area. The location of these profiles are drawn as thin white lines in Fig. 3. About 6260 km of RES profiles were manually analysed for the internal structure of the ice, namely the appearance and shape of internal layers, hyperbolas, as well as bottom reflections. The layering was detected each hundredth shot and at closer spacing where necessary. The layering was determined in the vertical marking beginning and end of the layering. Hyperbolas were detected in two different ways: hyperbolas at the base, which are often rather densely distributed, where assigned as horizontal sections in the radargram, whereas hyperbolas above the base were marked as indivual location, with a vertical coordinate representing the location of the crest. The beginning and end of areas where the bottom reflections were lost entirely, respectively discontinuous, were marked as well. Occasionally sparsly spaced hyperbolas still indicate

TCD
5, 1089–1122, 2011

some kind of bottom reflections. Special attention was given to the classification of the shape of the internal layering where it is not horizontally oriented. We have two classes which represent two clear patterns, down-welling and rippled, and one class that marks everything else that is not in agreement with typical horizontal layering (uneven). The latter class thus sums up different shapes, which could not be split in different classes. For these three classes we detected the horizontal and vertical extent of the respective regions in the radargram. The manual classification has been performed repeatedly and independent, so reproducibility is assured.

3 Synthesis of the data

The two radar systems are observing clearly two different parts of the ice shelf: the airborne 150 MHz RES is insensitive in the upper 50 m, whereas the 9.65 GHz TerraSAR-X signal penetrates presumably only 8–10 m, but definitely less than the theoretical 30 m (Ulaby et al., 1982). Thus we cannot quantitatively compare the two datasets. It is certainly a disadvantage that a radar survey with adequate frequencies resolving the upper 100 m is not available along the flight profiles. We focus in this study on the question if the near-surface structure, which we assume to be represented by the TerraSAR-X scenes, is in coincidence with structures at greater depth, indicating that the near surface structure is a consequence of the formation of structures at greater depth. Variation of the backscatter value potentially arise from inhomogeneities in the upper layers of firn, contributing to volume scatter or surface roughness that influences the scattering at the surface. These inhomogeneities might be hoar and ice layers, from drift snow forming wind crusts or summer surface melt that is more pronounced in depressions. Without firn core analysis a clear reason cannot be determined.

It has to be taken into account that the RES data were obtained in the presented region several years prior to the satellite data, so a displacement of several hundred metres between the two datasets occurs and thus a correlation coefficient of the location of the structure in RES and TerraSAR-X cannot be estimated. Therefore, we cannot contribute qualititatively to the discussion of Campbell et al. (2008), who have found no correlation between surface flow stripes of Kamb Ice Stream and signatures in radargrams crossing the ice stream.

The results of the classification are shown in Fig. 3a to d. The occurrence of internal layers (Fig. 3a) in the upper 30% of the profiles are displayed as light purple small dots, medium purple represents layering in the upper 60% of the ice column, while dark purple indicates layering that extends below that. Large dots beneath the small dots are marking a second block of internal layers at this location and the colour represents the lower boundary of the layered package. Due to the low flow velocity of the ice shelf, internal layers in the upper part are formed by accumulation on the ice shelf during the flow northwards.

Hyperbolas were found at various depth: in Fig. 3b the crests of those in the upper 30% of the ice column top are shown in light blue dots, between 30% and 60% in medium blue, from 60% to 90% in dark blue. The bold yellow line represent hyperbolas at the ice base, indicating sharp edges and crevasses. Basal hyperbolas are found almost everywhere in the ice stream and the western part of the ice shelf. In the latter an area close to the calving front appears to be free of hyperbolas. In this area we also found smooth horizontal layering. In the east, the shear margin and a boundary of about 50 km around the grounding line (also around the islands) exhibits basal hyperbolas.

Although the ice-water interface generally shows clear reflections (Fig. 3c), there are regions with missing (blue) and discontinuous (green) reflections. We propose that these kinds of reflections appear in areas where the base of the ice shelf is extremely rough. These types of reflections are located in the heavily rifted zone, close to the grounding line and at the margin of the ice stream.

Figure 3d compiles the different shape of the layers wherever they are not horizontally oriented. At some locations we found ripple-shaped layers (displayed in orange), typically the pattern extends over 15 m in the vertical and appears rather regular. With down-welling we denote areas where the layers are teared down almost to the base of the ice shelf (Fig. 4b at kilometre 10 is a typical example) over a distance of only few

TCD
5, 1089–1122, 2011

kilometres. The class uneven is then applied for areas where the layers are not plain horizontal and are neither rippled nor down-welled. In Fig. 4b at a distance of 0–4 km one example for this class can be found. Down-welling and uneven layers are solely found in the western rift zone, whereas rippled layering also appears in the ice stream. In the figures shown here we only display the appearance, or the horizontal location, of these classes, not the vertical distribution.

The ice thickness data, taken from the same profiles used for the classification of the zones and even more profiles measured at lower vertical resolution, allow to inspect the large scale structure of the ice shelf. The thickness varies strongly across the ice shelf: between 90 m at the ice front in the East and 866 m an the inflow of the Jutulstraumen. Figure 2b displays the obtained ice thickness in the western rift area in colour. The highly rifted area appears as a relatively thin area, with ice thicknesses less than 300 m, whereas the ice west and south-west of it, as well as the extension of the ice stream contains ice 300 to 500 m thick. East of Novyy Island another thin, less than 300 m thick region exists. The ice just next to the inflow of Jutulstraumen is extremely thin, barely 200 m thick. At the calving front, the thickness of the ice stream decreases in its northern fifty kilometres from 300–350 m to about 90 m at the western tip of Trolltunga. Along the western ice front, this gradient equals to a change from approximately 220 m thick ice decreasing at the northern most 30 km to about 90 m.

We will discuss the resulting zones (shown in Fig. 7) defined from surface characteristics and RES classification and their characteristics now in detail. Downstream the lee side of the rumple forms a long (about 55 km), feature-free, narrow distinct zone (Zone 8). Eastwards of this lee side-zone a band of alternating short and non-sharp surface structures can be found (Zone 9). This band, which is also well visible in Fig. 2, is another distinct zone. On the westward side of the lee-zone, we find an area which exhibits a regular pattern, consisting of 15 km long stripes aligned parallel to the flow direction (Zone 6). The large scale structures visible are more pronounced in the radar image in Fig. 2 as the sensor penetrates into the ice, while optical imagery (not shown here) rather suggests surface undulations then sharp-edged cracks.

TCD
5, 1089–1122, 2011

The detailed structure of the grounded zone is shown in Fig. 5. Its size is about 3 km × 3 km. The crevasse pattern and the absence of a dome-like surface elevation profile let us infer that this is an ice rumple. Ice rumples differ from ice rises by the fact that the ice flow is not divided around the obstacle, but the ice experiences a basal drag that leads to a rather minor distortion of the flow lines. As visible in Fig. 5a there is no division of the ice flow at the upstream end of the grounded area. Furthermore, Fig. 5b displays that the ice thickness does not vary significantly across the grounded area. This is a first indicator for an ice rumple. Figure 5c and d zoom into the grounded area and show its structure in a radar image (TerraSAR-X, c) and an optical image (ASTER, d). A comparison of these images reveals a field of fine scaled cracks across the grounded area, which undermines that the obstacle is overflown by ice. Thus, proving that this is an ice rumple. Nøst (2004) measured the water column thickness by means of seismics. This data shows, that south-west and north of the ice rumple the water depths is > 700 m, indicating a rough seafloor topography.

In order to get more insight into the vertical structure and the mechanism that caused the structure, we inspect the radargram along two cross sections that are displayed in Fig. 4a and b (for the locations of the profile see Fig. 2a) with a vertical exaggeration of 1:100. Figure 4a shows a radargram intersecting the large scale structures normal to the elongation (acquired 2004). The profile across the surface pattern reveals a very rough bottom topography. Blocks of undisturbed ice alter with hyperbolas. Although the flight direction is almost perpendicular to the surface pattern and flow direction, the alteration is visible only in a very compact manner, the profile exhibits down-welling of the internal layers at distinct locations. Figure 4b (taken in 2001) shows the down-stream area of this pattern and the intersection in an angle of about 45° allows a rather zoomed view. The down-welling of the internal layers, as well as the thinning of the layers is clearly visible. The vertical displacement in the down-wrapped areas is in the order of 50 m. The distance between the vertical layers is reaching the limit of the vertical resolution of the radar, which is 5–10 m. The crest of the down-welling coincidences often with a bottom undulation and basal crevasses. The thickness change in these area amounts about 20–30 m. Locations which show the down-welling exhibit horizontal layers at the uppermost ten to fifty metres.

Switching back to the broader view, the zone that exhibits the down-wrapping in the vertical has been assigned to be another distinct zone. The margins of this zone have in a first guess been derived from the radar imagery, but improved by the RES data, as the western boundary was chosen such that the alteration between layering/no layering was absent. About ~ 55 km downstream the ice rumple, east of the narrow band a field of fibre-like blocks of ice, which are partly bended, was identified (Zone 15). This area extends northwards to about the same latitude then the lee-zone and the narrow band.

Two further zones in the West were identified. Two are influenced by Novyy Island and two ice rises which are an extension of the Novyy Island. The southern zone is the lee side of a tiny ice rise close to Novyy Island (Zone 3). The second zone is most likely originated from outflow from Novyy Island into the ice shelf and the tidal displacement along the grounding line of Novyy Island. Its margins can well be identified in the radar imagery (Zone 4).

The 1969 Belgian Antarctic Expedition (van Autenboer and Decleir, 1969) reported a potentially grounded spot with an ice thickness larger than the surrounding area. The navigation of that expedition faced unfortunately some major problems, so that the precise location is not known. However, they suggested the ice shelf to be grounded at ~70.56° S, ~2.08° W. Thus we defined Zone 5 around that spot, supported by a RES section close by, that is shown in Fig. 4c. The RES profile passes the spot in 500 m distance at kilometre 35. While north of the spot in the first 30 km of the profile full layering and a smooth bottom are detected, further south sequences of disturbed layering and bottom crevasses followed by inclined layering and less crevassed bottom are surveyed, similar, but less pronounced as in Fig. 4a. The TerraSAR-X mosaic shows a smooth surface at this location.

The most northwards zone in the West is a region that exhibits two stripes in flow direction, with a distance of few kilometres, elongated in flow direction (Zone 13). Westwards of this stripe the ice appears structure free. At the margins of this zone, the basal reflections where lost, indicating a very rough base. Nicholls et al. (2006) surveyed this area with an autonomous underwater vehicle and discovered too, that the ice has a very rough bottom topography.

South of this zone we find a single large rift that is 29 km long and has a maximum width of ∼ 1 km. This rift is well visible also in ASTER images (not shown here), however, the radar imagery is advantageous here. The RES classification also reveals a change in properties across the rift (note that the RES data has been taken while the rift was further south). As this rift is separated from other structures, we assign this single feature an own zone (Zone 10).

Adjacent to the rift, a heavily crevassed, partly rifted area begins. We divided this area into three distinct zones, although there are no sharp boundaries between them. The structure of the entire area exhibits a clear boundary in the east towards the ice stream. The northernmost zone of the three (Zone 12) is characterised by wing-shaped rifts that are closely spaced, even interconnected on the western side. The southwestern side is less crevassed in the radar imagery. It exhibits rather extensions of the wing-shaped rifts and less dominant a similar pattern of undulations that we saw in the zone connected to the ice rumple. We assign this area a separate zone (Zone 14), as the damage visible on the surface is clearly less than in the real wing-shaped rift zone. The conjunction to the south is then the last of the three zones. The radar imagery shows again wing-shaped cracks, but with a lower density then northwards. This zone (Zone 17) is the direct extension of the zones generated by the ice rumple. The RES classification shows no internal layers in these areas and the zones have also a clear signature in the reflections: in some areas the bottom reflection is completely missing, in one profile discontinuous bottom reflections were found. Also hyperbolas in the interior are common.

The zones described above are located in the western rift area, which we aim to investigate. In order to understand the dynamics of this zone we need also to investigate the ice stream and as the dynamics of the ice stream is also influenced by its eastern margin, we go as far east as 1° E with the definition of zones. Beginning with the margin

TCD
5, 1089–1122, 2011

between the slow and fast moving ice masses in the west, we identified a zone which shows largely disturbed ice, fragments in form of blocks refrozen, which appears like a typical ice melange, directly north of Ahlmannryggen, where the Jutulstraumen leaves its lateral margins. This zone is narrowed down-stream and its surface characteristics changes as well, indicating that further north a zone of shear-margin type begins. The wedge shaped melange zone is defined as a single unit (Zone 18). It is has a counter part on the other side of the ice stream, which is discussed later in this section.

The already mentioned shear-margin kind region is adjoining northwards. This zone (Zone 16) is ~3 km narrow and ~155 km long. In the radar imagery this area extends up to the ice front at Trolltunga. It is interesting to mention, that this area is intersected by rifts from the western rift zone at one location in the middle part and twice from large rifts in the ice tongue far north. Except of two locations, the absence on continuous bed reflections is characteristic for Zone 16 and confirm the boundaries of this zone. At the northern end of Zone 16, we found an area that is confined in the South by the single large rift and in the West by Zone 13. The surface of this zone (Zone 11) exhibits an irregular pattern in the radar imagery. The RES data discloses gaps in the otherwise continuous basal reflections the north-south orientated rift which is also visible on the surface.

The fast moving area shows a complex pattern in the radar imagery, arising from the fast flow and the hinge zone at the grounding line. The radar imagery suggested zones along the entire length between grounding line and calving front. The RES classification of the hyperbolas reveals a difference between a western (Zone 19) and an eastern part, where basal hyperbolas are less frequent. In the TerraSAR-X mosaic, this part has a smoother surface and the structure of the surface is not aligned parallel to the flow as in Zone 19. The eastern part does, however, also not appear as one unit. Therefore we propose that there is a relative narrow band of similar structure (Zone 20), and a second wider band delimited by a shear margin (Zone 21). The middle part has less small scale cracks, but shows a pattern that is perpendicular to the flow, as if it would consist of single blocks. The definition of the zones in Jutulstraumen was also supported by flow modelling (which is otherwise not further discussed here), in which zones with a softening parameter were defined. In case the incorporation of an additional zone lead to more realistic flow fields, we kept the zone.

The transition between the fast ice stream and slow eastern part of the ice shelf is a rather wide zone ~ 18 km. It exhibits a dense field of tiny cracks in the TerraSAR-X mosaic (Zone 24). In the RES classification it appears as an area without internal layering, which is consistent from the characteristics of a shear margin. At the southern end of Zone 24, we find an area that is named Jutulgryta (Zone 22). Jutulgryta is known (Orheim et al., 1990a,b) to consist of an ice melange with icebergs, smaller fragments of meteoric ice, sea ice and intense melt ponds in summer. Therefore most profiles exhibit only discontinuous basal reflections. Furthermore, two potentially melange filled rifts at the eastern side of Trolltunga were identified in the TerraSAR-X mosaic.

4 Discussion

We hypothesize that the structure and dynamics of the western rift area, shown in Fig. 2, is dominated by two key areas: a small ice rumple at 71.2° S 1.85° W and Zone 15, formed downstream of Trollkjelneset. The internal structure of the RES profiles found in the various sub regions reveals the flow history of the single segments of the ice shelf.

The influence of the ice rumple on the ice shelf is clearly visible in the the radar imagery as well as in the RES profiles crossing the region around the ice rumple and Zone 15. However, a first guess would be that the ice rumple is responsible for the entire rift formation in the West, whereas a detailed inspection shows that it affects only a limited area and does not cause the formation of the major rift system further north. The fish-bone pattern of surface stripes starting at the ice rumple, which is more pronounced in the west than in the east, is intersected by larger rifts only in the west, where these cracks form in Zone 15. The dark stripes never transform downstream into wide crevasses; the zone never looses its integrity. It should be mentioned,

TCD
5, 1089–1122, 2011

that the southernmost, youngest stripes are less pronounced, than the following, older ones, pointing out, that the processes enhancing the dark stripes act not locally at the ice rumple, but downstream. Far downstream the dark stripes widen and become less pronounced (less contrast between the stripes and the surrounding ice), as snow accumulation covers the structure formed by the ice rumple and the TerraSAR-X penetration depth allows to penetrate only a small fraction into the structure.

By plotting the distribution of surface and internal hyperbolas in combination with the internal layering, the resulting pattern matches well with the surface characteristics detected by Terra-SAR-X. The low flow speeds in the western area of around 50–100 $\mathrm{m\,a^{-1}}$ correspond (taking the different acquisition periods into account) to a shift of about 6–10 shots in the radargram, which is in the range of uncertainty for the classes that are concerned with variations of internal layers, or about 40 pixels in the TerraSAR-X mosaic.

In order to shed more light on the influence of the ice rumple on the flow regime further, we discuss the RES profile upstream of the ice rumple (Fig. 4a). The rumple is located about 8.5 km away from this profile and a line drawn perpendicular to the flow direction would cross this profile at a distance of 1.8 km. Hence, this profile shows the far field of the local influence of the ice rumple. Internal layers exist over the entire depth. They are elongated horizontally in the upper part, whereas the lower half shows irregular undulations of the layers. Closer to the ice rumple, the upper layers are affected as well and get a wiggly structure. Further downstream, now at the same level as the ice rumple, the layering at the lower part is destroyed and first few hyperbolas in the lower part appear. At this location, the TerraSAR-X image shows the first slightly darker shaded stripe. It takes however 20 km until the layering in the upper part disappears and hyperbolas, as well as down-welling, appears. The RES profiles in the downstream area of the ice rumple exhibit several sequences of nearly undisturbed ice (Fig. 4a, 1.5 km to 3 km wide between distance 20 km to 110 km) with full layering and no hyperbolas, intersected by steeply orientated surface layering, hyperbolas in the upper part and strongly pronounced at the base.

This along-flow structure gives rise to the question, which processes take place in the vicinity of the ice rumple and cause this structure. We consider three processes to take place: crevassing at the upper and/or lower surface, stretching and basal melting. They might appear in different combinations with each other, leading to four hypotheses for the evolution of the pattern:

i. The sticky spot and the steep change in water column thickness to the west (Nøst, 2004), leads to local basal melting, that causes thinning in form of channels and subsequently the layers sink. The thinned sections are subjected to tensile stress, that leads to stretching and thus narrowing of the layers. No crevasses are formed at all.

ii. Basal shear stress at the ice rumples leads to built up of tensile stress at the base which episodically becomes critically, forming basal crevasses. These are intersecting the lower layers. Melting enhances the thinning, which causes the down-welling of the layers. Tensile stress leads then to stretching.

iii. Sea level and ice thickness change induce a stick/slip motion, where during the stick mode stretching of the downstream area takes place and during slipping the layers remain undisturbed. The basal tensile stress remains sub-critical and thus the basal topography would exhibit undulations instead of basal crevasses.

iv. Cracks are formed at the surface and the base of the ice symmetrically, as indicated by fracture mechanics, leading to intersection of layers at the surface and base. Stretching thins the distance between the un-intersected layers and again, adjustment to hydrostatic equilibrium leads to sinking of the layers.

The former two hypotheses rely on basal melting, while the latter two are purely deformational and independent of the ability of the ocean for melting the bottom of the ice shelf. The dataset we are using gives no information at all if basal melting occurs. Nevertheless, hypothesis (i) describes a process that would not lead to a formation of new crevasses, whereas the RES sections show new hyperbolas, indicating cracks.

TCD
5, 1089–1122, 2011

Thus we see (i) as falsified. Hypothesis (ii) would require basal crevasses: the radar section show that upstream the rumple region, basal crevasses exist and the base of the ice shelf was never transfered to a smooth surface by melting. Nevertheless, the basal crevasses were obviously small, as the apex of the hyperbolas is at the lower boundary. Downstream the ice rumple new hyperbolas in the lower part, but up to about 30% of the thickness from the base, are created. This indicates deep crevasses or crevasses that were melted out. The ice is clearly thinner at those locations, making an additional basal melting likely. An intersection of layers in the lower part is not clearly visible, however, small spots with layers remain in between the hyperbolas. However, it can neither be proven nor disproven.

The basal undulations suggested by hypothesis (iii) can be disproven by the RES sections. A hyperbola is supposed to be formed where a sharp crack exists, whereas moderate basal undulation cannot produce a basal hyperbola. There are clearly cracks and crevasses at the lower surface. However, the distance between the location of down-welling and near surface hyperbolas, changes with along the profile perpendicular to the ice flow (Fig. 4a) and the distance between the dark stripes in Figs. 2 and 5 is not constant, although the pattern is partly regular. This makes a change in the basal regime at the ice rumple on the timescale of decades likely.

Hypothesis (iv) proposes surface crevasses, thus we try to test this hypothesis by investigating the location of hyperbolas and surface cracks visible in the TerraSAR-X images. The RES sections reveal 10–15 km downstream the location of the rumple first hyperbolas with an apex at about 30% of the ice thickness below the surface. At the same locations, hyperbolas at about 1/2 to 2/3 of the depth exist, as well as hyperbolas of about 15% above the lower surface. Coincidently, the near surface layers are down-welled. Below the apex of the uppermost hyperbolas no layering exists. The absence of near surface hyperbolas further upstream let us suggest that hyperbolas are formed close to the location we observe them and thus about 10–15 km downstream the ice rumple. They are thus a secondary step of the impact of the basal shear stress over the rumple. However, hypothesis (iv) requires the coincidence of surface and basal

TCD
5, 1089–1122, 2011

crevasses. The hyperbolas are clearly not located at the surface, nor is there any hint in TerraSAR-X images that surface crevasses in coincidence with the dark stripes exist (whereas few narrow, short cracks on the sides of the dark strips exist, possibly arising from bending stresses). The crests of the hyperbolas are so far below the surface, that we cannot claim them to be surface crevasses. They seem to be formed below the ice surface, potentially the hyperbolas are originated by a basal crevasse that starts at the lee zone of the rumple, propagating westwards as well as upwards. This is also undermined by the fact that the crests of the hyperbolas further upstream on the RES section are located deeper, thus the cross section shows a slice of the flow history, in which the propagation reached different vertical levels. It remains however unclear why the cracks have not propagated through the ice shelf entirely, but were arrested just about 120 m below the surface.

These stripes of down-welling remain in Zone 6 in the flow history for the subsequent 85 km in an area which is dominated by tensile stress, before they experience shear at the northernmost part of Zone 6 where this zone merges with Zone 17. The tension stretches the ice at the locations where the ice was intersected by the basal crevasses more than the undisturbed units and widens these zones. This is visible in the radar imagery in Fig. 2, as well as in the RES section in Fig. 4a. The signature in the radar section in Fig. 4b becomes more complex, as the flight direction is no longer perpendicular to the flow direction. Kinks in the internal layers appear as in Fig. 4b at distance 3 km, wherever the RES sections cross a dark stripe in the TerraSAR-X scenes in directions other than perpendicular to the flow direction. The kinks and down-welled zones, which appear much wider in the non-perpendicular sections thus represent a zoom into the structure of the dark stripes. These sections also allow us to conclude that the pattern all over the dark stripes in Zone 6 are in general similar.

In conclusion a new hypothesis with the verified components from the above listed hypothesis can be formulated: when the ice passes the ice rumple, basal crevasses are formed, which penetrate laterally eastwards and westwards. They extend in the profile only in the lower third of the ice column. Downstream the cracks propagate vertically,

TCD
5, 1089–1122, 2011

either due to load at the crack tip arising from the water pressure, or tensile stress that overcomes the cryostatic contribution in size still arising from the basal shear stress. The locations of the cracks represent sections of thinner ice, potentially enhanced by basal melting, and thus the horizontal layers are welled down. Additionally the trough in the surface elevation leads to intensified snow accumulation by wind-blown snow. This causes the darker zones in the TerraSAR-X images. Further downstream the ice experiences tension, leading to stretching of the thinner sections, that results in narrowing of the distance of the internal layers and widening of the sections. Figure 6 displays this in form of a cartoon, showing the basal crevasses, the surface structure and the down-welling at the side of the block.

In order to complete the discussion of the effect of the ice rumple we are now considered with the zone east of the lee zone, Zone 9. What applies for Zone 6 also holds for Zone 9, nevertheless its lateral extent is obvious much less. We suggest that this is due to an inhomogeneous flow unit, that originates at the grounding line. This flow unit arrests the crack propagation. In the flow history both zones, Zone 6 and 9, never loose their integrity, the basal crevasses never penetrate up to the surface. At few locations crevasses from other areas propagate into these areas.

The loss of the lateral margin at Ahlmannryggen in Zone 15 rises the tensile stress and leads to crack formation at the eastern margin of this zone. The cracks propagate laterally and generate individual blocks of undisturbed ice that are connected to each other only to a minor extent. They experience at the area of the formation of the blocks only tensile stress, which is evident as the ice is not bended in any direction. Further downstream the merging of the ice masses build up compressive stress. The compressive stress leads to a separation of the crevassed western ice mass into individual fibres. The fibres become bended and even folded. The built up of shear stress increases the separation of the fibres, thus a propagation from crevasses to rifts, and thus to distortion of some plains. From there on, the structure of the western rift area is formed by the shear stress between the slower moving western part and the fast ice in the centre. In contrast to wing cracks, that are formed when rifts are experiencing

TCD
5, 1089–1122, 2011

compressive stress, the orientation of the bended ends of the rifts here is opposite and thus points out that the rifts are deformed under shear stress. The northernmost, large rift (Zone 10) exemplifies this situation best.

Severe shearing between the fast flowing region of the Jutulstraumen and the heavily crevassed neighbouring regions on its western side causes the loss of basal reflections. Although Zone 16 appears in the radar imagery as a narrow band that reminds on a shear zone, it is not decoupling the flow in the central from the west. The same applies to Zone 18, which nourishes Zone 16. Both zones are strong enough to sustain the shear and transmit it to the western part of the ice shelf. We claim that the lateral stretching of Jutulstraumen after it passed the narrow valley, visible as a widening of the cross section of the ice stream in the radar imagery, is the reason for this coupling. In the broader perspective, the reason for the western rift system is the fact that no typical shear margin is formed along the western margin of the ice stream. With a real shear margin that decouples the two parts of the ice shelf, such an area full of large rifts and crevasses could not have been evolved.

Although it is not directly related to the western rift zone, we add here a discussion of Zone 5, a location previously discussed by van Autenboer and Decleir (1969). The north-western part of the ice shelf, which appears rift free in the radar imagery (except very close to the calving front) high accumulation rates (Rotschky et al., 2007) and low flow speeds lead to the formation of internal layering. In this area Zone 5 is situated, that was suggested to be grounded. Zone 5 is located close to a RES section obtained in 2001, shown in Fig. 4c. Approximately at kilometre ~35 this profile passed in 500 m distance the suggested grounded spot. The RES profile shows lots of internal hyperbolas, presumably arising from basal crevasses. Although there is some ripple structure in the internal layers below the surface visible, the upper layers are unaffected and there is only a minor change in the ice thickness. Surface depressions that accumulate wind-blown snow and thus appear in the radar imagery as darker spots, are not formed. Consequently, this area does not leave a signature in the radar imagery. Hence, a structure-free surface in the TerraSAR-X does not allow to assume, that the

TCD
5, 1089–1122, 2011

A. Humbert and D. Steinhage

Title Page
Abstract | Introduction
Conclusions | References
Tables | Figures
◀| |▶
◀ ▶
Back | Close
Full Screen / Esc
Printer-friendly Version
Interactive Discussion

internal structure does not consist of down-welling, uneven or rippled layers. It does on the other hand allow to infer, that the ice thickness is not changing on short spatial scales. For the dynamics of the ice flow, this grounded spot means that the flow speeds are reduced to a certain amount. It is however interesting to note, that the spot is almost invisible in imagery, although the 50 m ice thickness change from the Belgian Expedition suggests a small dome-like structure visible. The RES data shown here, confirms the findings of van Autenboer and Decleir (1969), as the obtained thickness change is in our dataset 46 m.

5 Conclusions

In total twenty-three 150 MHz RES profiles surveyed with a 60 ns pulse and one with 600 ns obtained between 1996–2008 we found down-welling of internal layers, as well as rippled and uneven internal layers, partly with kinks and steep gradients. The channelised flow of Jutulstraumen into the ice shelf destroyed the internal layering in the ice stream, so that deep layering appears only in the slow flowing areas in the of the ice shelf. The majority of the hyperbolas were located at the base or in the lower third of the ice shelf, indicating generally a rough bed. In the vicinity of large rifts and at the margin of the ice stream the basal reflections were lost.

A mosaic of TerraSAR-X radar scenes, acquired between 2008 and 2010 in stripmap and ScanSAR mode, covering the entire ice shelf, serves as a base for the detection of units with identical properties. Because the X-band radar signal penetrates into the upper 8–10 m metres of the ice, these images allow a much more detailed identification of spatial units, even though crevasses and flow stripes might be covered by fresh snow, than purely optical sensors.

The morphological interpretation of the combination of RES and X-band radar imagery data lead to the identification of 26 structurally distinct domains. RES sections reveal that the surface characteristics detected in the TerraSAR-X data are a consequence of the vertical structure and therefore always represent inhomogeneous ice.

TCD
5, 1089–1122, 2011

The structure and dynamics of the western rift area, shown in Fig. 2, is caused by (i) a small ($3 \times 3\,\text{km}^2$) ice rumple at 71.2° S, 1.85° W and (ii) a zone with fibre-like ice blocks that is formed at the junction between Jutulstraumen and the slower, thinner western part ice shelf:

i. The rumple changes the structure of the ice shelf through the entire thickness (see Fig. 4a and b) in its vicinity and 25 km, downstream over width of about 10 km. Although the vertical structure exhibits strong deformation of the internal layers and also hyperbolas throughout the thickness, it never looses entirely its integrity and does not contribute to the formation of rifts.

ii. The inflow in the western part of the ice shelf looses its lateral constraint at Ahlmannryggen, where crevasses were formed. The contact of the eastern end of this flow unit with Jutulstraumen exerts compressive stress that leads to separation into blocks, which are later on bended and folded like fibres. We infer that this process is the origin of the western rift zone. Northwards, the rifts are prone to shear, leading to wing formation and growth.

Although we found a narrow band between the ice stream and the western rift zone, this band does not prohibit the transmission of shear on the ice masses in the west. The western rift zone is thus also a consequence of a strong mechanical coupling, or an absence of decoupling, of the two merging parts of the ice shelf.

Acknowledgements. This study was supported by the German Research Foundation (DFG) under grants HU 1570/2-1 and the cluster of excellence CliSAP at the KlimaCampus of the University of Hamburg. The TerraSAR-X images were provided by the German Aerospace Center (DLR) under proposal LAN0013. We thank Robert Metzig (DLR) for the support in acquiring the TerraSAR-X images. ASTER images were provided by the European Space Agency under IPY AOPOL.4032. The radio echo sounding data was partly acquired in the VISA-Project (DFG Research Grant Jo191/8-1&2). A. H. want to thank Roland Warner (ACE and CRC, Hobart, Australia), Dietmar Gross (TU Darmstadt), Robert Metzig (DLR) and Dana Flouricou (DLR) for fruitful discussions. We thank Johannes Lohse for support of the classification of the RES data.

TCD
5, 1089–1122, 2011

References

Campbell, I., Jacobel, R., Welch, B., and Pettersson, R.: The evolution of surface flow stripes and stratigraphic folds within Kamb Ice Stream: why don't they match, J. Glaciol., 54, 421–427, 2008. 1095

Davis, C. H. and Poznyak, V. I.: The depth of penetration in Antarctic firn at 10 GHz , Geosci. Rem. Sens., 31, 1107–1111, 1993. 1092

Fritz, T. and Eineder, M.: TerraSAR-X Ground Segment Basic Product Specification Document, Tech. rep., DLR, 2009. 1092

Humbert, A.: The thermal regime of the Fimbul Ice Shelf, Antarctica, Ann. Glaciol., 51, 56–64, 2010. 1090

McClain, E. P.: Eleven year chronicle of one of the world's most gigantic icebergs, Mariners Weather Log, 22, 328–333, 1978. 1091

Nicholls, K. W., Abrahamsen, E. P., Buck, J. J. H., Dodd, P. A., Goldblatt, C., Griffiths, G., Heywood, K. J., Hughes, N. E., Kaletzky, A., Lane-Serff, G. F., McPhail, S. D., Millard, N. W., Oliver, K. I. C., Perrett, J., Price, M. R., Pudsey, C. J., Saw, K., Stansfield, K., Stott, M. J., Wadhams, P., Webb, A. T., and Wilkinson, J. P.: Measurements beneath an Antarctic ice shelf using an autonomous underwater vehicle, Geophys. Res. Lett., 33, L08612, doi:10.1029/2006GL025998, 2006. 1100

Nixdorf, U., Steinhage, D., Meyer, U., Hempel, L., Jenett, M., Wachs, P., and Miller, H.: The newly developed airborne RES-system of the AWI as a glaciological tool, Ann. Glaciol., 29, 231–238, 1999. 1093

Nøst, O. A.: Measurements of ice thickness and seabed topography under the Fimbul Ice Shelf, Dronning Maud Land, J. Geophys. Res., 109, C10010, doi:10.1029/2004JC002277, 2004. 1098, 1104

Orheim, O., Hagen, J. O., and Østerhus, S.: Studies on, and underneath, the ice shelf Fimbulisen, Norsk Polarinstitutt. Meddelser, 113, 59–73, 1990a. 1091, 1102

Orheim, O., Hagen, J. O., Østerhus, S., and Sætrang, A. C.: Glaciologic and oceanographic studies on Fimbulisen during NARE 1989/90, FRISP Rep., 4, 120–131, 1990b. 1091, 1102

Rotschky, G., Holmlund, P., Isaksson, E., Mulvaney, R., Oerter, H., Van den Broecke, M. R., and Winther, J.-G.: A new surface accumulation map of western Dronning Maud Land, Antarctica, from interpolation of point measurements, J. Glaciol., 53, 385–398, 2007. 1108

Rott, H., Sturm, K., and Miller, H.: Active and passive microwave signatures of Antarctic firn by means of field measurements and satellite data, Ann. Glaciol., 17, 337–343, 1993. 1093

Swithinbank, C. W. M., McClain, P., and Little, P.: Drift Tracks of Antarctic Icebergs, Polar Rec., 18, 495–501, 1977. 1091

Ulaby, F. T., Moore, R. J., and Fung, A. K.: Microwave Remote Sensing, Active and Passive, vol. II, Artech House Inc., 1982. 1095

van Autenboer, T. and Decleir, H.: Airborne radio-glaciological investigations during the 1969 Belgian Antarctic Expedition, Société belge de géologie, de paléontologie et d'hydrologie Bulletin, 78, 87–100, 1969. 1099, 1108, 1109

Vinje, T. E.: Frift av Trolltunga i Weddellhavet, Norsk Polarinstitutt. Arbok, p. 213, 1975. 1091

TCD

5, 1089–1122, 2011

The rift zone of the Fimbul Ice Shelf

A. Humbert and D. Steinhage

Discussion Paper | Discussion Paper | Discussion Paper | Discussion Paper |

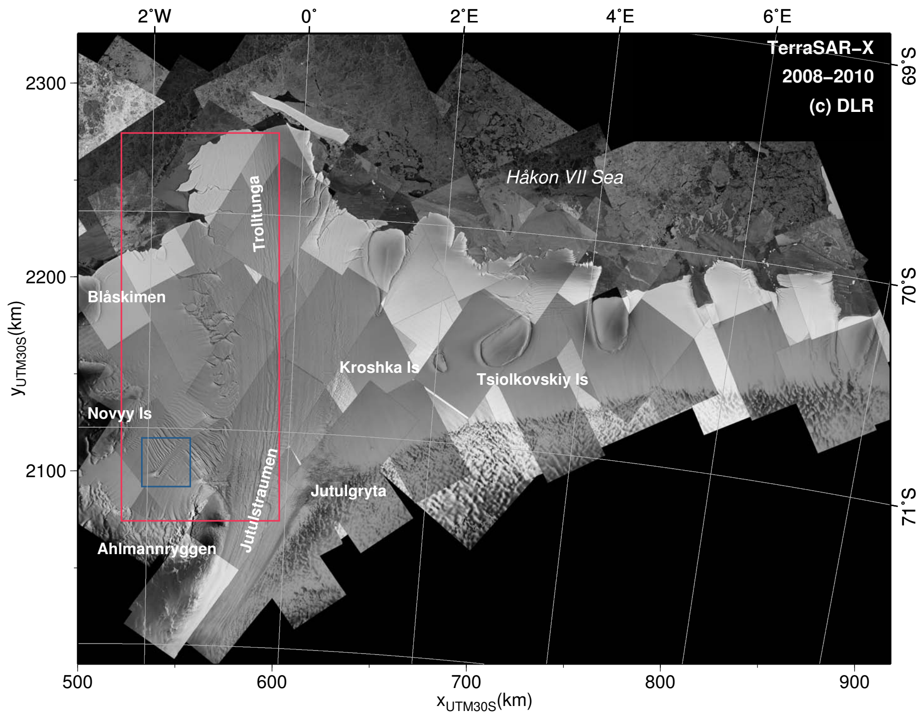

Fig. 1. Map of Fimbulisen showing TerraSAR-X mosaic derived from images in stripmap mode and ScanSAR mode acquired between 2008 and 2010.

TCD
5, 1089–1122, 2011

A. Humbert and D. Steinhage

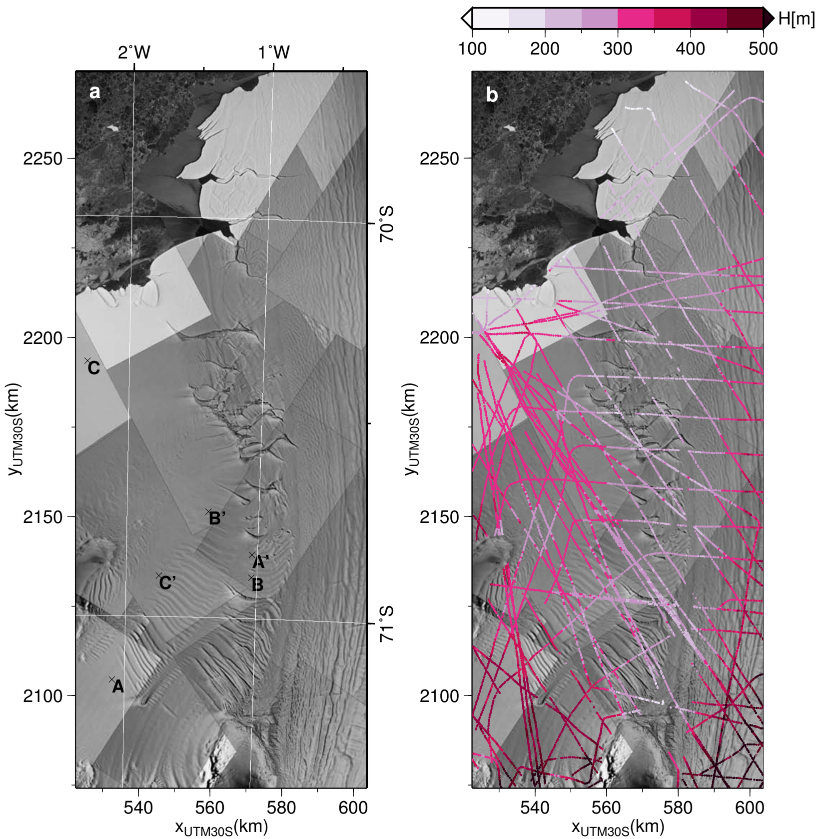

Fig. 2. Panel **(a)**: subset of the TerraSAR-X mosaic showing the western rift area of Fimbulisen, as well as large parts of the extension of Jutulstraumen. Panel **(b)**: same as left, with superimposed ice thickness along RES profiles in colour.

TCD
5, 1089–1122, 2011

Title Page
Abstract | Introduction
Conclusions | References
Tables | Figures
◀I | ▶I
◀ | ▶
Back | Close
Full Screen / Esc
Printer-friendly Version
Interactive Discussion

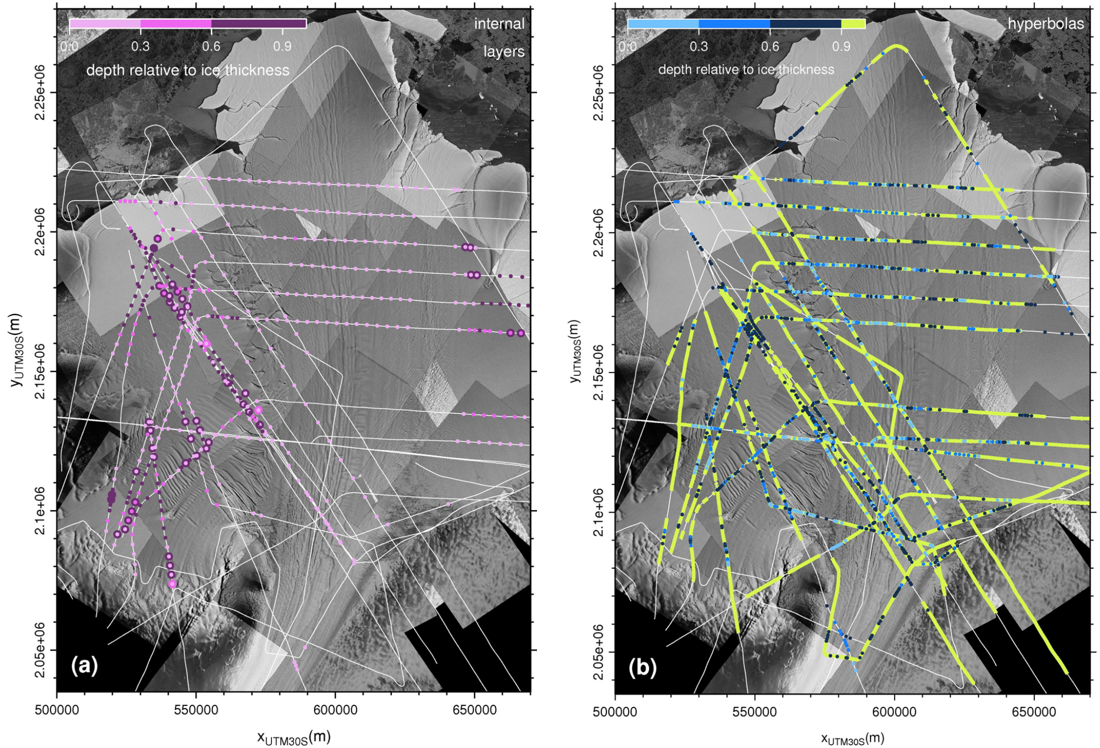

Fig. 3. First two of four maps displaying the RES classification of the internal structure superimposed on the TerraSAR-X mosaic. **(a)** Internal layers: light purple and medium purple denotes layers down to 30%, respectively 60% of the ice thickness, dark purple full layering. Large dots beneath the small dots are marking a second block of internal layers. **(b)** Hyperbolas: light blue denotes hyperbolas located at the top, yellowish at the bottom, blue in the interior of the ice shelf and dark blue denotes hyperbolas at top and interior locations.

TCD

5, 1089–1122, 2011

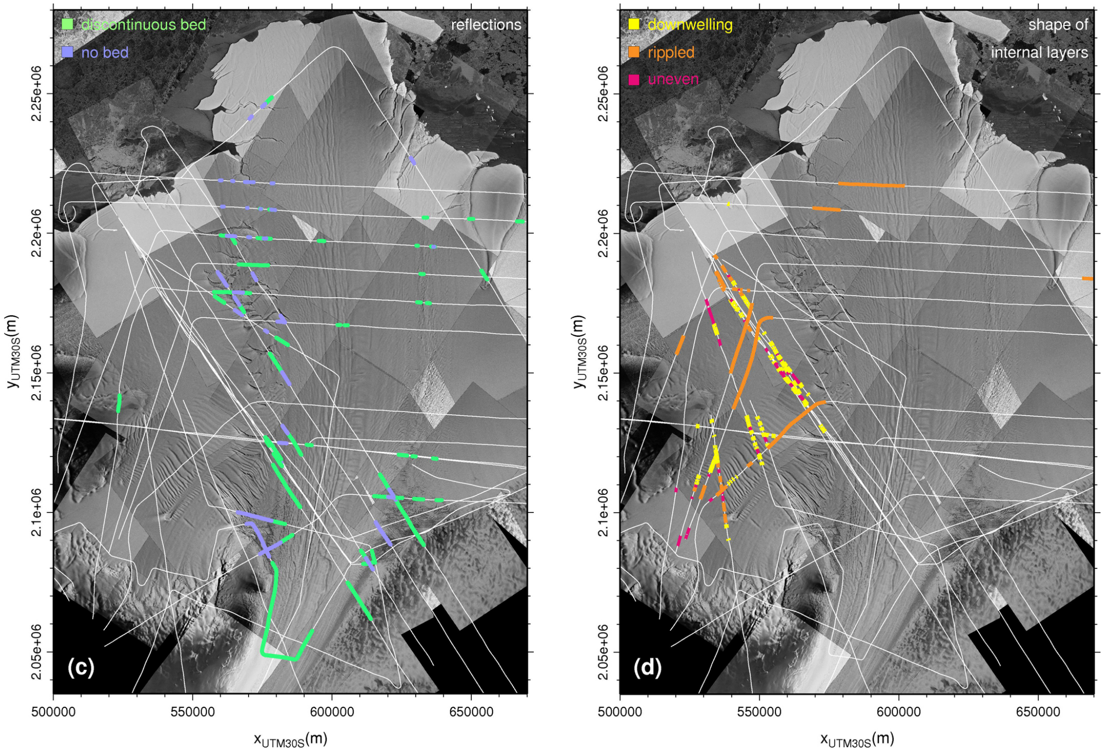

Fig. 3. Second two of four images displaying the RES classification of the internal structure superimposed on the TerraSAR-X mosaic. **(c)** Reflections: blue missing bottom reflection, green discontinuous reflections. **(d)** Shape of internal layers: down-welling in yellow, rippled shape in orange and uneven in pink.

TCD
5, 1089–1122, 2011

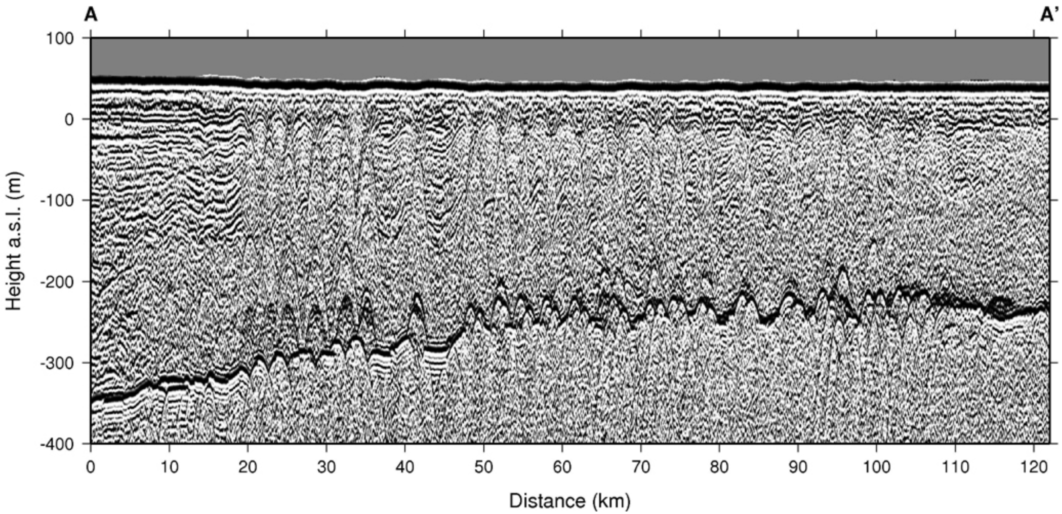

Fig. 4a. Radargram showing a 60 ns profile acquired in 2004 reaching from A to A′ (locations of are shown in Fig. 2a).

TCD
5, 1089–1122, 2011

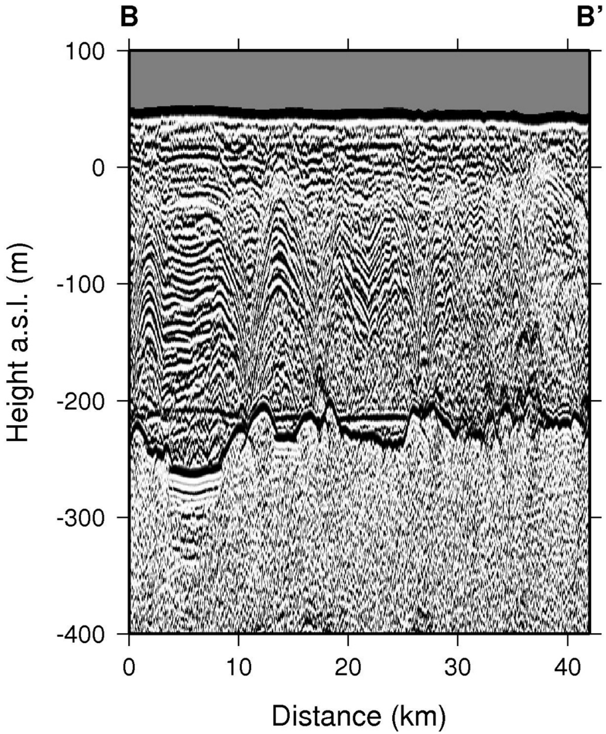

Fig. 4b. Radargram showing a 60 ns profile acquired 2001 ranging from B to B′ (locations of are shown in Fig. 2a). The horizontal line at approximately −200 m is a multiple reflection between aircraft and surface.

Discussion Paper | Discussion Paper | Discussion Paper | Discussion Paper |

TCD

5, 1089–1122, 2011

The rift zone of the Fimbul Ice Shelf

A. Humbert and D. Steinhage

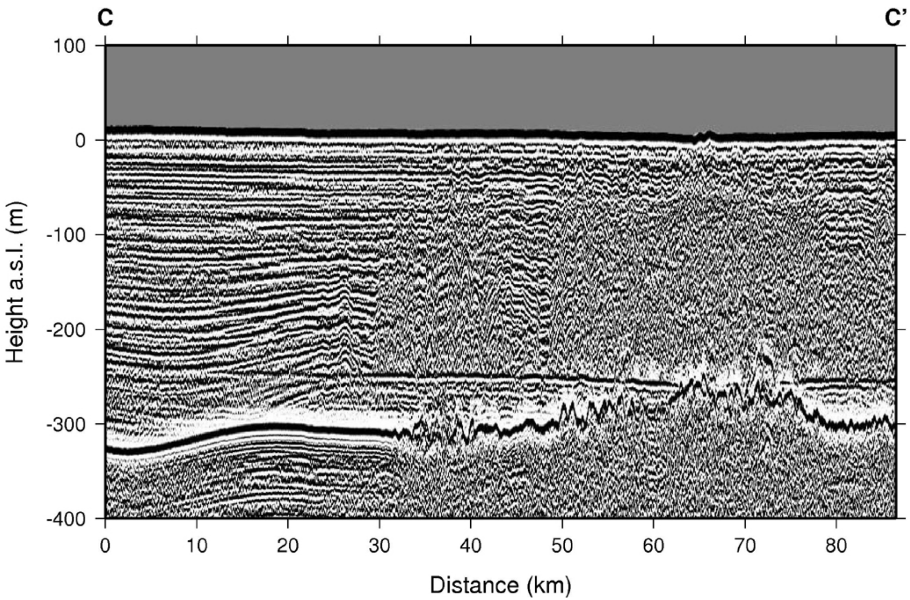

Fig. 4c. Radargram showing a 60 ns profile acquired in 2001 ranging from C to C′ (locations of are shown in Fig. 2a).

TCD
5, 1089–1122, 2011

A. Humbert and D. Steinhage

Title Page
Abstract Introduction
Conclusions References
Tables Figures
◂ ▸
Back Close
Full Screen / Esc
Printer-friendly Version
Interactive Discussion

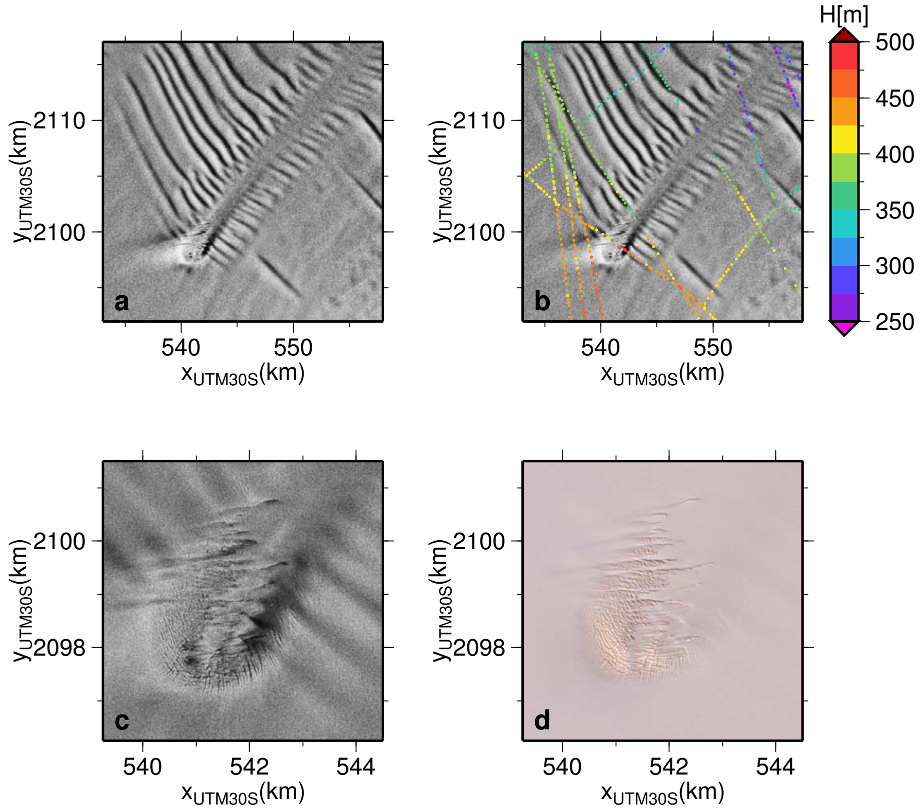

Fig. 5. Details of the ice rumple: **(a)** TerraSAR-X ScanSAR image taken on 5 November 2009. **(b)** same as **(a)** with superimposed RES ice thickness data. **(c)** TerraSAR-X stripmap mode image from 25 November 2008. **(d)** ASTER image of the same area as **(c)** from 6 August 2007.

TCD

5, 1089–1122, 2011

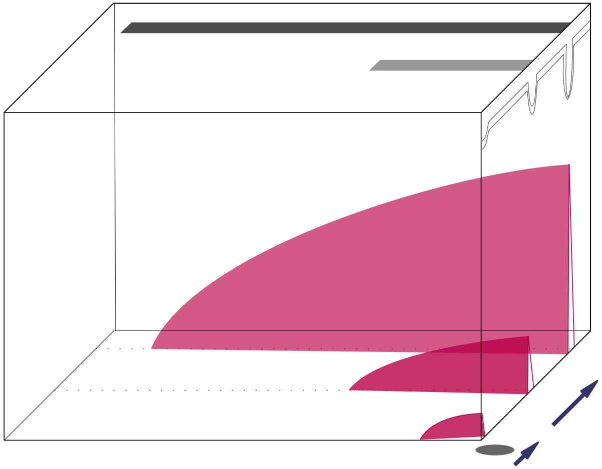

Fig. 6. Sketch illustrating the origin of the surface and internal structure north-west of the ice rumple shown Fig. 5.

TCD
5, 1089–1122, 2011

A. Humbert and D. Steinhage

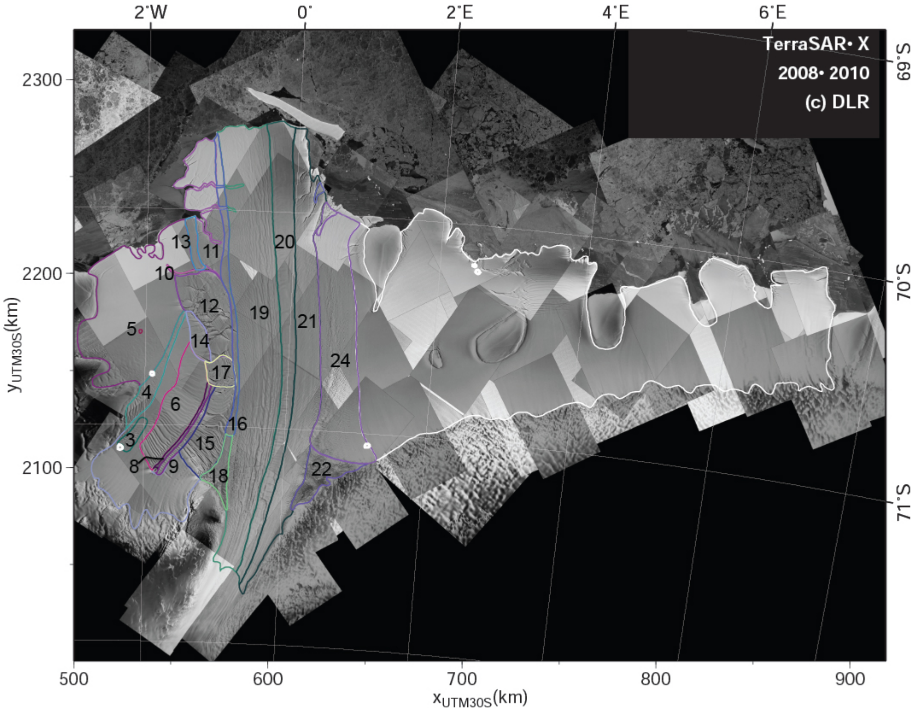

Fig. 7. TerraSAR-X mosaic and the sub domains defined from structural mapping of TerraSAR-X images and the RES classification.

TCD
5, 1089–1122, 2011

The rift zone of the Fimbul Ice Shelf

A. Humbert and D. Steinhage

Title Page
Abstract
Introduction
Conclusions
References
Tables
Figures
◀
▶
Back
Close
Full Screen / Esc
Printer-friendly Version
Interactive Discussion